

Application of semiconductor nanomaterials in cancer theranostics

Mehrnaz Mostafavi^{1*}, Jaleddin Ghanavi², Mahtab Shaabani³, Hamed Asadi⁴ and Mahsa Alizadeh⁵

¹Department of physics, Faculty of Paramedical Sciences, Shahid Beheshti University of Medical Sciences, Tehran, Iran; ²MRC, NRITLD, Shahid Beheshti University of Medical Sciences, Tehran, Iran; ³Department of internal medicine, Loghman hakim Hospital, Shahid Beheshti University of Medical Sciences, Tehran, Iran; ⁴Department of internal medicine, Loghman hakim Hospital, Shahid Beheshti University of Medical Sciences, Tehran, Iran; ⁵Department of physics, Faculty of Paramedical Sciences, Shahid Beheshti University of Medical Sciences, Tehran, Iran

ABSTRACT

Cancer theranostics, which aims to integrate diagnostics and therapy for cancer treatment, has benefited greatly from recent advancements in nanomaterials. This study focuses on the most recent advancements in cancer theranostic techniques using quantum dots, silica nanoparticles, and carbon-based nanomaterials. Over the last decade, responsive nanocarriers made from these nanomaterials have shown promise in cancer-specific theranostics. Several experiments in cell and mouse models have suggested their underlying therapeutic efficacy; however, comprehensive and long-term in vivo clinical evaluations are undoubtedly expected to make these bench-made materials compatible in real-world settings.

Keywords: Theranostics; Silica nanoparticles; Carbon-based nanomaterials; Quantum dots

INTRODUCTION

Latest developments in nanomaterials have supported cancer theranostics, which aims to combine diagnostics and therapy for cancer patients. This research looks at the latest progress of many cancer theranostic techniques that use quantum dots, silica nanoparticles, and carbon-based nanomaterials. Several studies in cells and mice models have shown that they are therapeutically effective; however, rigorous and long-term in vivo clinical experiments are needed to ensure that these bench-made materials are consistent in real-world settings [1-4].

We provide an overview of numerous theranostic techniques developed using inorganic silica and carbon-based nanomaterials for various cancer therapies in this study. Silicon and sulfur are the two most common elements on the planet, making them two of the most significant nonmetallic compounds in human life

In this article, we provide an overview of a number of theranostic techniques for different cancer therapies that have been produced using inorganic silica and carbon-based nanomaterials. Since silicon and sulfur are two of the most abundant elements on the earth, they are two of the most important nonmetallic compounds in human life.

Silicon is a key component in electronics and has been used in a broad range of practical developments. Carbon is the basis for life's

chemistry, while silicon is a key component of electronics and has been used in a wide range of practical developments. Among the different types of nanomaterials developed in recent years, research on nanocarbons such as carbon nanotubes, graphene, fullerene, nanodiamond, and carbon nanoparticles (CNPs) has emerged as a booming field. [5-9] Apart from carbon nanotubes, the other fullerene family has certain unique physicochemical properties that could be used to develop new DDS for cancer theranostics. [10-14] Quantum-sized (1-10 nm) fluorescent CNPs are another promising carbon-based nanomaterial for cancer therapy. In both in vitro and in vivo clinical applications, fluorescent CNPs have shown environmental friendliness, low toxicity, and low cost over semiconductor QDs. Because of their unique properties, they hold promise for applications such as drug delivery, biosensing, and bioimaging [15-19].

Properties of quantum dots nanoparticle (QDs) as theranostics agents

Quantum dots (QDs) are used for the bioimaging purposes due to their unique features. Their conjugation with homing and therapeutic agents results in multimodal nanosystems. The main drawback of QD-based theranostics is their intrinsic toxicity because of cadmium ions. To attain safe and biocompatible QDs, different types of Cadmium-free QDs have been engineered. Quantum

*Correspondence to: : Mehrnaz Mostafavi, Department of physics, Faculty of Paramedical Sciences, Shahid Beheshti University of Medical Sciences, Tehran, Iran, Tel: 989124766808, E-mail: mz_mostafavi@sbmu.ac.ir

Received: April 11, 2021; Accepted: April 21, 2021; Published: April 27, 2021

Citation: Mostafavi M, Ghanavi J, Shaabani M, Asadi H, Alizadeh M (2021) Application of semiconductor nanomaterials in cancer theranostics. J Nanomed Nanotech. 12: 563.

Copyright: ©2021 Mostafavi M, et al. This is an open-access article distributed under the terms of the Creative Commons Attribution License, which permits unrestricted use, distribution, and reproduction in any medium, provided the original author and source are credited.

dots are semiconductor crystals in the nano-scale range of 2–10 nm. They exhibit unique photoluminescence characteristics. QDs possess strong photoluminescence with high molar extinction coefficient values. They are the best candidates for cell labeling and detection of cancer biomarkers. strategies have been developed to reduce their toxicity and enhance their biocompatibility [20].

Protein–QD hybrid nano-theranostics play a crucial role in bioimaging applications. QDs can be hybridized with proteins via either chemical coupling or physical entrapment. Zein-ZnS QD nano-hybrid structures could be utilized for drug delivery of compounds such as 5-fluorouracil. Using proteins for hybridization of QDs could be a potential strategy to prolong their systemic circulation, increase their physical stability, enhance their tumor targetability and reduce their toxicity, we say. We conclude that using proteins to hybridize QDs with proteins could be an effective strategy to extend circulation and enhance tumor penetration, among other benefits. The author would like to make clear that the study was on cancer cells treated with QDs and not QDs.

One of the most important approaches for QD surface functionalization is their encapsulation into a layer of amphiphilic diblock or triblock copolymer. Volsi et al. functionalized QDs with lipoic acid (LA), PEG and FA to form an amphiphilic copolymer (PHEA-LA-PEG-FA) that self-assembled into micelles in aqueous medium. The fluorescent nanoprobes demonstrated high internalization into MCF-7 breast cancer cells and localized mainly in the cytoplasm. Anti-EGFR nanobodies were conjugated to the surface of the QDs to target EGFR-over-expressing cancer cells. The QD-based theranostic micelles led to tumor regression in a triple negative breast cancer mouse model [21].

Intravenously injected carbon quantum dots selectively accumulate in human tumour xenografts in mice. The functionalized quantum dots structurally mimic large amino acids and can be loaded with aromatic drugs. They enabled near-infrared fluorescence and photoacoustic imaging of the tumours and a reduction in tumour burden. Semiconductor quantum dots (QDs) are atomic light-emitting nanocrystals constructed from semiconductor materials with unique optical, electrical, and chemical properties used in biomedical research (e.g., size-tunable light emission, high photobleaching resistance, strong absorption, a sharp and symmetrical fluorescence peak, solid and stable emission, and high quantum yield). [23,24] As fluorescence resonance energy transfer (FRET) pairs of fluorescent organic dyes, QDs have been used in theranostic

agents as targeting Ligands such as antibodies, peptides, or small molecules [25,26]. Quantum dots can be used both in vivo and in vitro, as shown by the following three scientific applications.

Application of QDs in vitro studies

Combining diagnosis and therapy using graphene quantum dots (GQDs) is a prime focus and challenge for researchers. GQDs is a new shining star among various fluorescent materials, which has acclaimed fame in a short duration in materials science and the biomedical field. This Review provides an update for the scientific community to plan and expand advanced theranostic horizons in BC using GZDs [27].

Bagalkot et al. created a ternary system [QD-Apt(Dox)] made up of a QD, an aptamer (Apt), and the small molecular anticancer drug doxorubicin (Dox) and investigated its use for simultaneous in vitro targeted imaging, therapy, and drug release sensing (Figure 1 (a) and (b)). A10 RNA aptamers were coupled to QD surfaces as targeting inducements, and Dox was applied to the stem region of the aptamers. Two donor–quencher pairs of FRET resulted from QD and DOX interactions with DOX and RNA, respectively. LNCaP prostate adenocarcinoma cells were incubated for 0.5 hours at 37°C with 100 nM QD-Apt(Dox) conjugate before being imaged immediately and 1.5 hours later (Dox). Both QD and Dox fluorescence signals were small in LNCaP cells at the start of operation, but fluorescence of both QD and Dox increased significantly over 1.5 hours (Figure 1 (c) and (d)).

Figure 1.(a) Diagram of the QD-Apt(Dox) Bi-FRET unit. In the first step, the A10 PSMA aptamer is used to surface functionalize the CdSe/ZnS core-shell QD. When Dox is intercalated within the A10 PSMA aptamer on the surface of QDs, the QD-Apt(Dox) is formed, and both QD and Dox fluorescence is quenched by a Bi-FRET operation. (b) QD-Apt(Dox) conjugates have a one-of-a-kind uptake into target cancer cells via PSMA-mediated endocytosis. As Dox is released from the QD-Apt(Dox) conjugates, both QD and Dox fluorescence is restored (the “ON” state), allowing for synchronous fluorescent localization and killing of cancer cells. (The letters A, B, C, and D stand for A, B, C, and D, respectively.) PSMA- expressing LNCaP cells were incubated for 0.5 h at 37°C with 100 nM QD-Apt(Dox) conjugates, washed twice with PBS buffer, and then incubated for (c) 0 h and (d) 1.5 h at 37°C. The overlay of Dox and QD fluorescent is depicted in the lower right images of each panel, with Dox and QD fluorescent depicted in

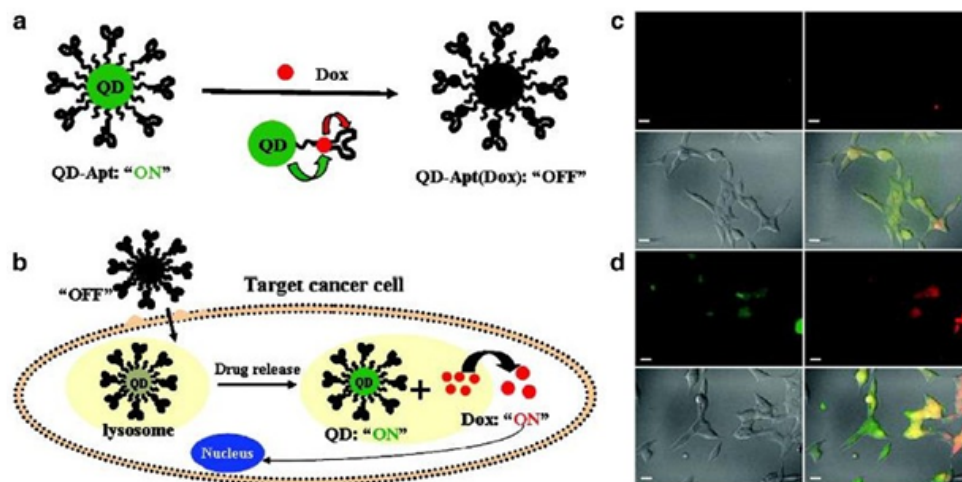


Figure 1: (a) Diagram of the QD-Apt(Dox) Bi-FRET unit. In the first step, the A10 PSMA aptamer is used to surface functionalize the CdSe/ZnS core-shell QD. When Dox is intercalated within the A10 PSMA aptamer on the surface of QDs, the QD-Apt(Dox) is formed, and both QD and Dox fluorescence is quenched by a Bi-FRET operation. (b) QD-Apt(Dox) conjugates have a one-of-a-kind uptake into target cancer cells via PSMA-mediated endocytosis.

red and green, respectively. This article has been published with the permission of Ref [28]. As a result, Dox was released from the conjugate, inducing the fluorescence of both QDs and Dox, and thereby acting as a drug release tracker *in vitro*. The *in vitro* cellular cytotoxicity of the QD-Apt-(Dox) conjugate was calculated using the MTT assay, and the findings were similar to those of free Dox and QD alone. In cell lines, QD had no significant cytotoxicity, while free Dox and the QD-Apt-(Dox) conjugate were treated similarly, meaning that Dox was gradually liberated from the conjugate following intracellular absorption by cell lines [28].

Application of QDs in vivo studies

Nurunnabi et al., who prepared functionalized quantum dots, gave a short description of the use of quantum dots *in vivo*. The near-infrared QDs were encapsulated in a mixture containing PEGePCDA and PCDAe Herceptin conjugates to change their water solubility and target-specific properties (Figure 2).

Structure of micelles containing near-IR QDs. (a) PEG, PCDA, and Herceptin chemical structures. (b) Micelles filled with near-IR QDs have a cross-linked structure. With permission from Ref [29], this article has been reprinted.

The NPs (near-IR QDs-loaded micelles) demonstrated a feasible tumor targeting approach and applicable therapeutic effects when measured on an MDA-MB-231 tumor platform. Tumor growth

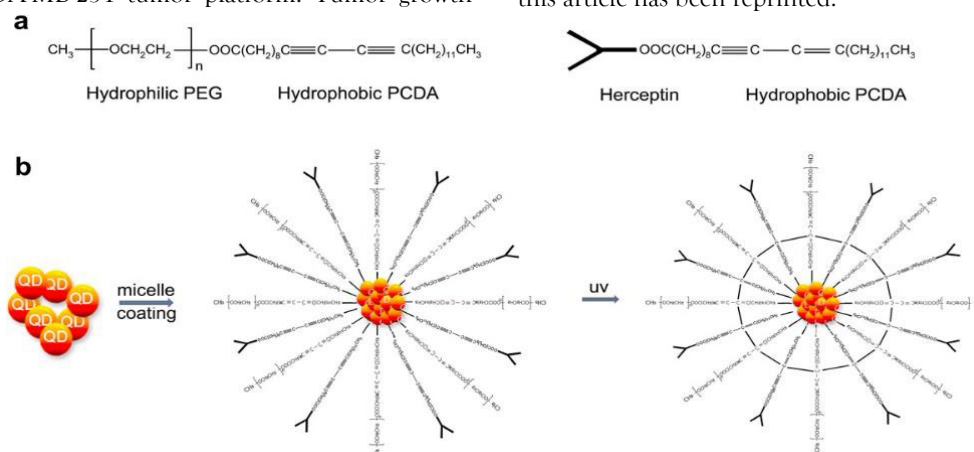


Figure 2: Structure of micelles containing near-IR QDs.

(a) PEG, PCDA, and Herceptin chemical structures.

(b) Micelles filled with near-IR QDs have a cross-linked structure. With permission from Ref [29], this article has been reprinted.

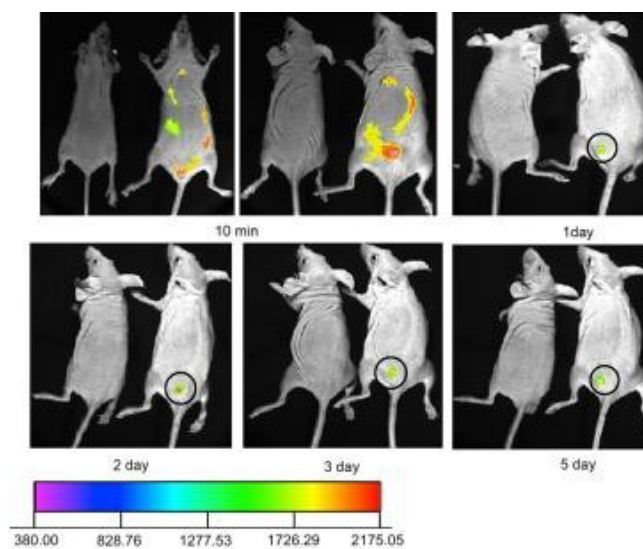


Figure 3: Five-day non-invasive fluorescence imaging of tumor-bearing mice.

inhibition by NPs was checked, and tumor volume was decreased by 79 percent after 5 days of treatment with near-IR QDs-loaded micelle compared to before treatment. The IR QDs-loaded micelles could be a good choice for cancer therapy since there was no mortality due to toxicity during treatment or weight loss in mice. Using non-invasive fluorescence imaging, the biodistribution of near-IR QDs-loaded micelles in tumor-bearing nude mice (MDA-MB-231) was investigated (Figure 3). Micelles containing near-IR QDs is inserted into tumor-bearing nude mice intravenously. The NPs rapidly spread around the animal's body and tumor. Ten minutes after the nanoprobe were injected, visible fluorescence patterns were seen in the body. 24 hours after the nanoprobe were injected, the images revealed a small volume of core deposition (10 mg/kg). At this time, there was a strong signal at the tumor site. Both nanoprobe concentrations were observed only in the tumor area on the fifth day. It shows that non-target organs (heart, liver, and stomach) cleared nanoprobe quickly, suggesting that nanoprobe were not harmful to these healthy organs [29].

Figure 3: Five-day non-invasive fluorescence imaging of tumor-bearing mice. The concentration of near-IR QDs in the micelles was 10 mg/kg. Micelles containing near-IR QDs were inserted into the tail veins of MDA-MB-231 tumor-bearing mice. The intensity bar depicts the fluorescence intensity frequency of the tumor side. The tumor is shown by the circle. With permission from Ref [29], this article has been reprinted.

Application of QDs in vivo and in vitro studies

The tumor targeting and anti-tumor effects of 5-fluororacil (5-FU) primed, folic acid (FA) targeted Mn-ZnS quantum dots encapsulated with chitosan (CS) biopolymer (QDs) were investigated by Ibrahim Birma Bwatanglang and colleagues (Figure 4). 5-FU is a cancer-fighting drug that is injected into a vein. The aim of both of these studies was to reduce the drug's side effects.

Figure 4. (a) Schematic Structure of 5-FU loaded folate MN:ZnS nanocomposite. (b) Structure. (b) FTIR contrast of 5-FU and 5-FU@FACS-Mn:ZnS composite bands. With permission from Ref [30], this article has been reprinted.

MTT assays were used to assess cell viability in two different treatment groups. The cytotoxicity of MDA-MB-231 breast cancer cells was studied after they were treated with 5-FU (pure drug) and 5-FU@FACS-Mn:ZnS hybrid with various concentrations of both 5-FU and 5-FU@FACS-Mn:ZnS, as well as standard MCF-10 cells from a different culture. The viability of breast cancer MDA-MB231 cells was decreased more than in the 5-FU only case when abnormal cells were treated with 5-FU@FACS-Mn:ZnS at a concentration greater than 125 g/mL. The 5-FU drug, on the other hand, destroyed more than half of MCF-10 cells, while 78 percent of MCF-10 cells incubated with 5-FU@FACS-Mn:ZnS survived (Figure 5). The efficacy of FA-conjugated QDs in increasing the intracellular absorption and selectivity of 5-FU in comparison to pure 5-FU therapy is due to these results.

Figure 5. In vitro cell viability experiments with (a) MDA-MB231 cancer cells and (b) MCF-10 normal breast cells after treatment with FACS-Mn:ZnS, 5-FU, and 5-FU@ FACS-Mn:ZnS. With permission from Ref. [30], this article has been reprinted.

In this study, the researchers looked at the treatment effectiveness of 5-FU, Mn:ZnS, and 5-FU@ FACS- Mn:ZnS in tumor-bearing mice (body weight, tumor volume and tumor weight). The body weight of those who received Mn:ZnS was found to be slightly lower than that of those who received the other treatments. The 5-FU@ FACS-Mn:ZnS grades, on the other hand, had the highest level of treatment and the least amount of animal weight loss. In two groups treated with 5-FU@ FACS-Mn:ZnS and pure

5-FU, tumor volume reduction was found to be about 21% and 13%, respectively. Furthermore, unlike the untreated groups, the Mn:ZnS-treated groups did not show any reduction in tumor volume [39].

Figure 6. On (a) mean body weight, (b) tumor volume, and (c) tumor weight, the effects of 5-FU, Mn:ZnS, and 5-FU@ FACS-Mn:ZnS were compared. (d) depicts a cultivated tumor with (I) no treatment, (II) 5-FU, and (III) 5-FU@FACS-Mn:ZnS treatment. With permission from Ref. [30], this article has been reprinted.

Properties of Carbon nanotubes (CNTs) as thranostics agents.

Over the last two decades, carbon nanotubes (CNTs) have piqued interest in biomedical applications [31,32]. Because of their bonding mechanisms (sp² and sp³), CNTs have intrinsic optical properties such as fluorescence and photo acoustic emission, making them ideal for biological imaging [33]. The NIR Semiconducting CNTs, in fact, have an NIR photoluminescence that makes them suitable for use as NIR fluorescent contrast agents [9,17]. Furthermore, CNTs with a high absorption potential have been widely used in cancer PTT. [19] Because of their ability to cargo both attacking ligands and chemotherapy agents, CNTs have been used in vitro and in vivo. Furthermore, the use of CNTs in a living organism necessitates simple fictionalization to reduce toxicity and non-specific binding. PEGylation (polyethylene glycolylation) becomes the method for enhancing CNT pharmacokinetics and biocompatibility [34].

Review of in vivo treatments of CNTs

Part (A)

Zhuang Liu et al. investigated in vivo single-walled carbon nanotubes (SWNT) packed with DOX (SWNT-DOX). Figure 1 shows the schematic structure and AFM of the SWNT-DOX complex. (See Figure 7).

Figure 7. (a) The SWNT-DOX matrices are shown. (b) An AFM image of the SWNT-DOX complexes. The SWNT-DOX conjugates are 2–3 nm in diameter and 100 nm in length on average. The scale bar is 250 nm. This article has been reprinted with permission from Ref. [35-37].

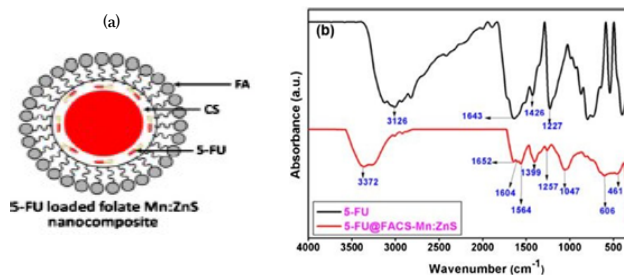


Figure 4: (a) Schematic Structure of 5-FU loaded folate MN:ZnS nanocomposite. (b) Structure. FTIR contrast of 5-FU and 5-FU@FACS-Mn: ZnS composite bands.

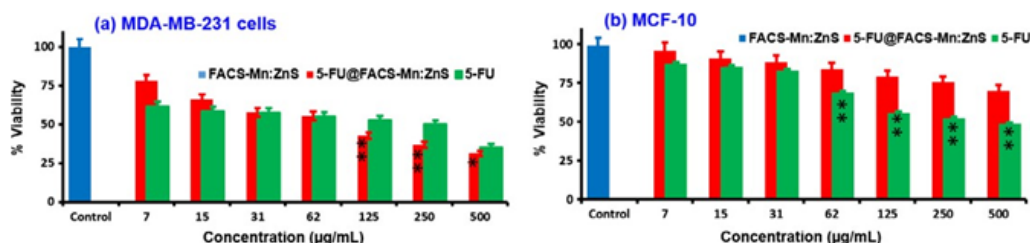


Figure 5: In vitro cell viability experiments with (a) MDA-MB231 cancer cells and (b) MCF-10 normal breast cells after treatment with FACS-Mn:ZnS, 5-FU, and 5-FU@ FACS-Mn:ZnS.

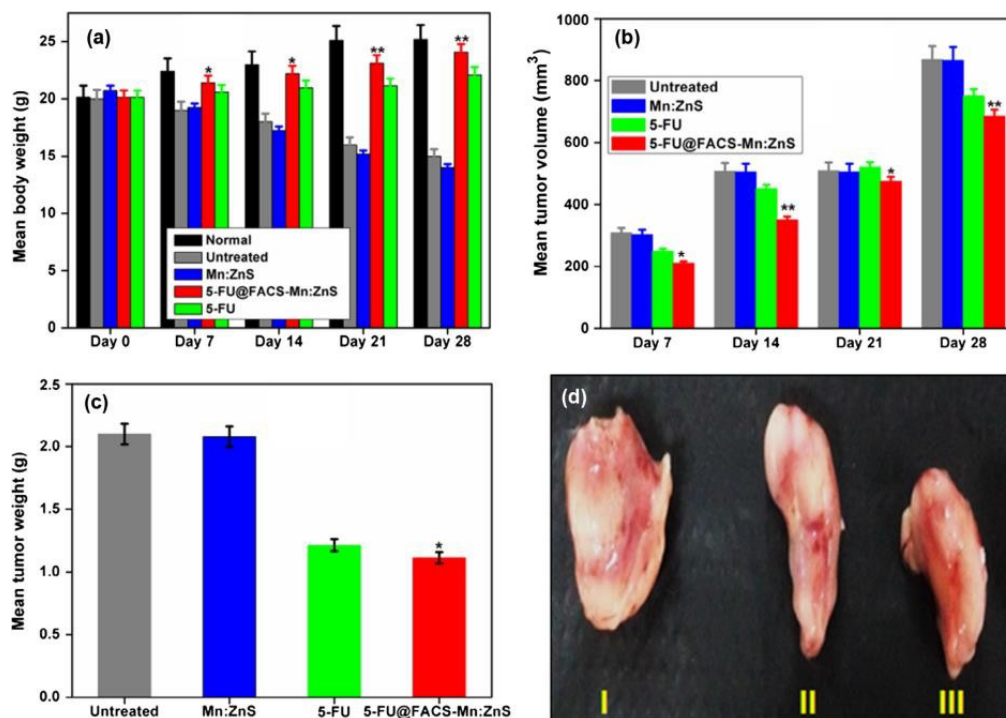


Figure 6: On (a) mean body weight, (b) tumor volume, and (c) tumor weight, the effects of 5-FU, Mn:ZnS, and 5-FU@FACS-Mn:ZnS were compared. (d) depicts a cultivated tumor with (I) no treatment, (II) 5-FU, and (III) 5-FU@FACS-Mn:ZnS treatment.

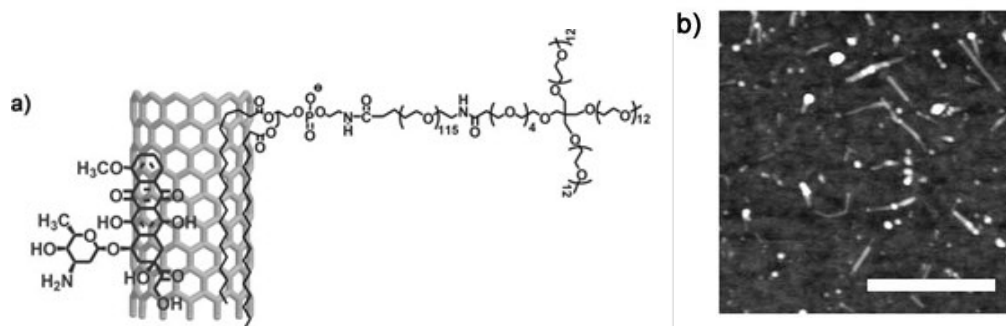


Figure 7: (a) The SWNT-DOX matrices are shown. (b) An AFM image of the SWNT-DOX complexes. The SWNT-DOX conjugates are 2–3 nm in diameter and 100 nm in length on average. The scale bar is 250 nm. This article has been reprinted with permission from Ref.[37].

Such SWNT-DOX was examined in SCID mice carrying Raji lymphoma xenografts. SWNT-DOX (n=10), free DOX (n=10), or DOXIL (n=10) were provided once a week to SCID mice with Raji lymphoma xenograft tumors. In the second week, two mice died. They found that the SWNT-DOX had a much higher medicinal efficacy and was less toxic than DOX and DOXIL. The tumor sizes of each population were determined during therapy. In related terms, the SWNT-DOX treated group inhibited tumor development rather than the free DOX group (Figure 8 (a)). The SWNT-DOX population had steady weight and no mortalities as compared to the free DOX therapy (Figure 8 (b)). SWNT-DOX thus outperformed free DOX in terms of therapeutic efficacy and toxicity [37].

Figure 8. (a) Tumor sizes in untreated (n=7), 5 (mg kg⁻¹) free DOX treated (n=10), 5 (mg kg⁻¹) Doxil treated (n=5), (mg kg⁻¹) SWNT-DOX treated (n=10), and 10 (mg kg⁻¹) SWNT-DOX treated (n=10) mice were measured throughout treatment. (b) Representative images of mice from different populations were taken at the end of therapy. Mice are slightly smaller after being granted free DOX. With Ref. [46]'s permission, [37] this article has been reprinted.

Part (B)

Zhang Liu et al. conjugated paclitaxel (a cancer chemotherapy drug) to branched polyethylene glycol chains on SWNTs. SWNT-PTX conjugate was studied and compared to other therapies in a 4T1 murine breast cancer model in mice. They found that SWNT-PTX therapy had a longer blood circulation half-life than the other drugs and had a higher tumor uptake. In a murine 4T2 breast cancer models, researchers concluded that using SWNT had apparent less toxicity than clinical Taxol in suppressing tumor development [38].

Figure 9. (A) Example of PTX conjugation of SWNT functionalized by branched PEG chains in phospholipids. (B) SWNT UV-VIS-NIR spectra before and after conjugation with PTX. (C) Tumor growth curves of 4T1 tumor-bearing mice treated with various therapies. With permission from Ref. [38], this article has been reprinted.

Properties of Silica nanoparticles as theranostics agents

As theranostic agents, NPs with the potential to circulate around the body hold a lot of promise [39]. The high specific surface area of mesoporous silica is suitable for drug cargo in medical applications

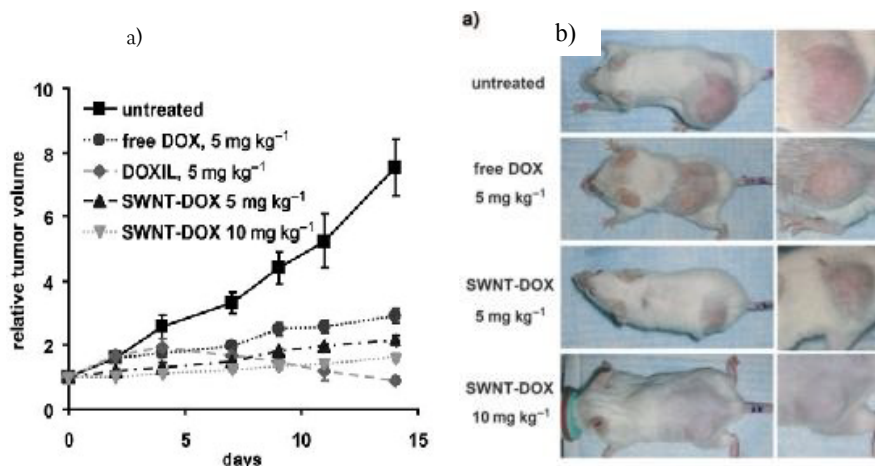


Figure 8: (a) Tumor sizes in untreated ($n=7$), 5 (mg kg^{-1}) free DOX treated ($n=10$), 5 (mg kg^{-1}) Doxil treated ($n=5$), (mg kg^{-1}) SWNT-DOX treated ($n=10$), and 10 (mg kg^{-1}) SWNT-DOX treated ($n=10$) mice were measured throughout treatment. (b) Representative images of mice from different populations were taken at the end of therapy.

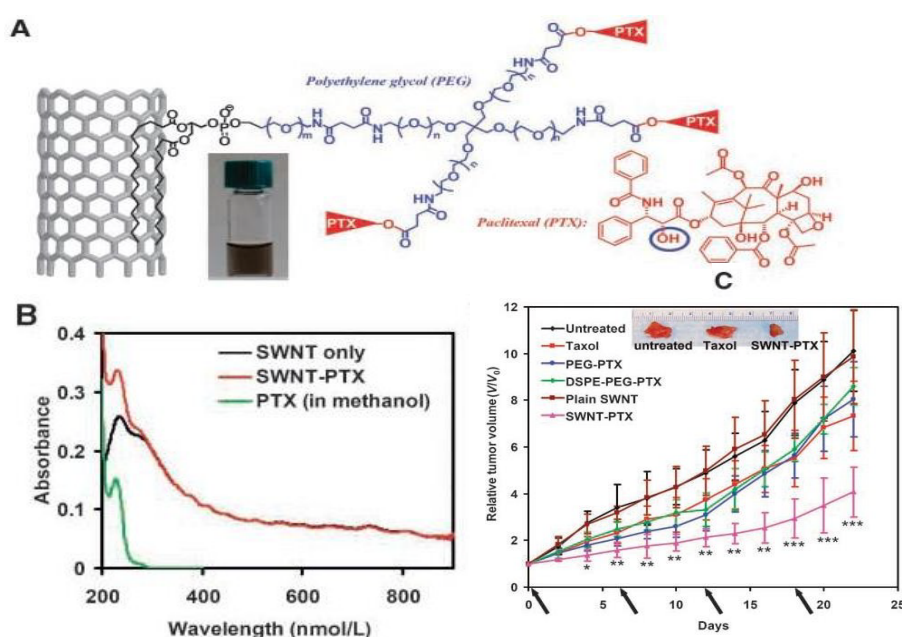


Figure 9: (A) Example of PTX conjugation of SWNT functionalized by branched PEG chains in phospholipids. (B) SWNT UV-VIS-NIR spectra before and after conjugation with PTX. (C) Tumor growth curves of 4T1 tumor-bearing mice treated with various therapies.

[40]. It is also possible to control the size and morphology of silica nanoparticles during the synthesis process [41,42]. IONPs, Au NPs, and QDs can be used to encapsulate a wide range of functions while preserving their physical properties such as magnetic and optical properties. [43-45]

A Review of silica nanoparticle based theranostic agents

A reasonable beneficial NIR active capability was obtained by altering the shape of pure gold NPs. For X-ray/CT imaging as a diagnostic modality and dual-mode PTT and radiation therapy (RT) as a therapeutic modality, folic acid was conjugated to less expensive silica modified GNRs (GNR-SiO₂-FA) (Figure 10).

Figure 10. (a) Synthetic procedure of GNR-SiO₂-FA. (b) A TEM representation of GNR-SiO₂ and the electron diffraction pattern that corresponds. (c) GNR-SiO₂-FA TEM image. With permission from Ref. [46], this article has been reprinted.

In vitro RT effects on cancer cells: On MGC803 cells, the effects of in vitro radiation therapy were investigated. After being

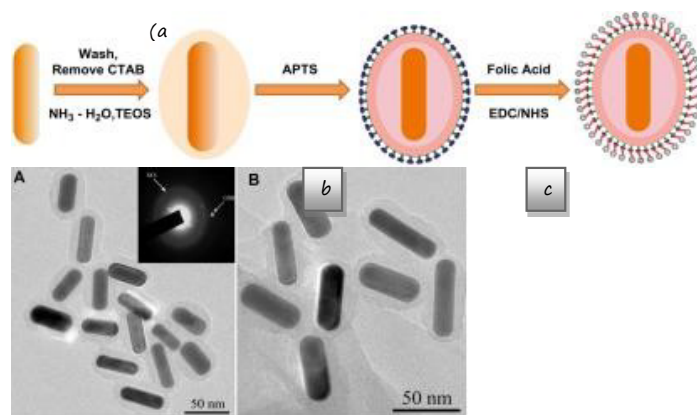


Figure 10: (a) Synthetic procedure of GNR-SiO₂-FA. (b) A TEM representation of GNR-SiO₂ and the electron diffraction pattern that corresponds. (c) GNR-SiO₂-FA TEM image.

incubated with varying amounts of GNR-SiO₂-FA, MGC803 cells were irradiated with linear accelerators. The nanoprobe's dosage was increased from 0.625 to 12.5 μg . The cells were divided into

two groups: one was exposed to X-rays, while the other was not. Cell viability decreased as the concentration of GNR-SiO₂-FA rose only in the case of X-ray irradiation, as seen in (Figure 11). Cell viability was almost equal in the first and second groups [46].

In vitro PTT effects on cancer cells: PTT was performed on MGC803 cells that had been incubated with 12.5 μ M GNR-SiO₂-FA for 24 hours at 37°C. Where the laser was irradiated, all of the cells died; however, the cells remained alive within the laser's limits. Dark-field images of MGC803 cells revealed that the cell membrane ruptured as the irradiation time increased (Figure 12).

Figure 12. (A) MGC803 cells on the laser spot, (B) MGC803 cells on the laser spot's boundary, and (C, D) MGC803 cell dark-field images after irradiation. With permission from Ref. [46], this article has been reprinted.

X-ray/CT dual-modality tumor imaging using GNR-SiO₂-FA: In

vivo X-ray images of mice after subcutaneous injection without and with GNR-SiO₂-FA suspended in PBS were obtained at different time points (0h, 2h, 6h, 8h and 24h). More bright images were collected with a longer injection time. It's likely that the cause is due to the presence of PBS, which caused a high level of GNR-SiO₂-FA absorption in the body (Figure 13).

Figure 13. In vivo X-ray imaging of mice following subcutaneous injections of GNR-SiO₂-FA (left) and GNR-SiO₂-FA (right) at various time points. (A) A photograph of mice; (B, C, D, E, F) an X-ray shot taken at 0 h, 2 hours 6 hours, 8 hours, and 24 hours. Respectfully, With permission from Ref. [46], this article has been reprinted.

In vivo CT photographs of nude mice after subcutaneous injection of GNR-SiO₂-FA suspended in PBS showed that the injection site's Hounsfield Units (HU) values were higher than those of other tissues (Figure 14).

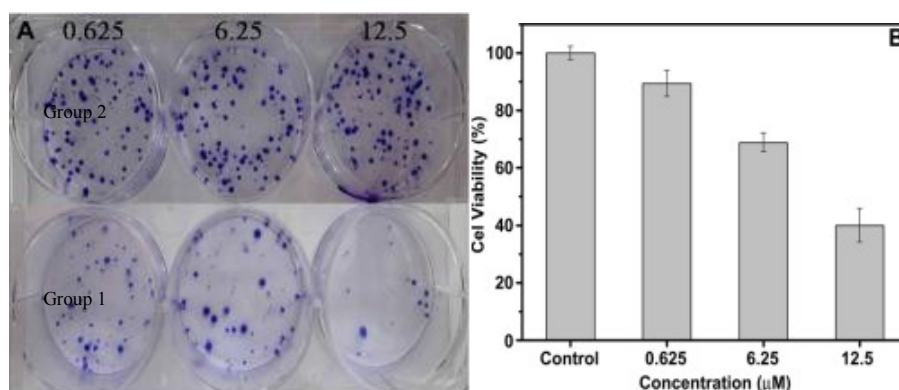


Figure 11: The proliferation photographs (A) and cell viability (B) of MGC803 cells incubated with 100 μ L of varying concentration of GNR-SiO₂-FA for 24 h upon 6 Gy of X-ray irradiation.

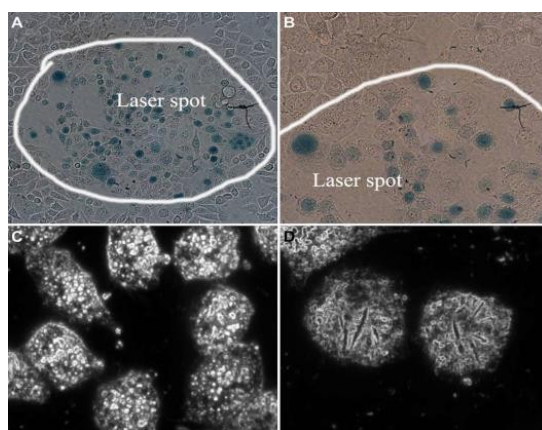


Figure 12: (A) MGC803 cells on the laser spot, (B) MGC803 cells on the laser spot's boundary, and (C, D) MGC803 cell dark-field images after irradiation.

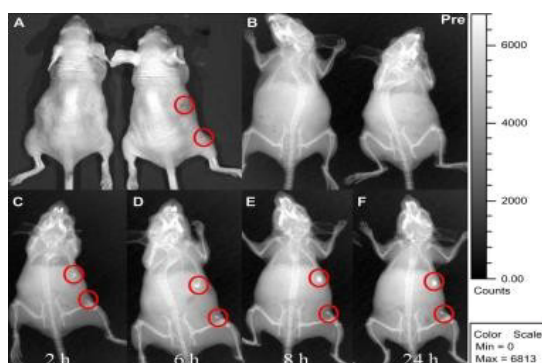


Figure 13: In vivo X-ray imaging of mice following subcutaneous injections of GNR-SiO₂-FA (left) and GNR-SiO₂-FA (right) at various time points. (A) A photograph of mice; (B, C, D, E, F) an X-ray shot taken at 0 h, 2 hours 6 hours, 8 hours, and 24 hours. Respectfully, With permission from Ref. [46].

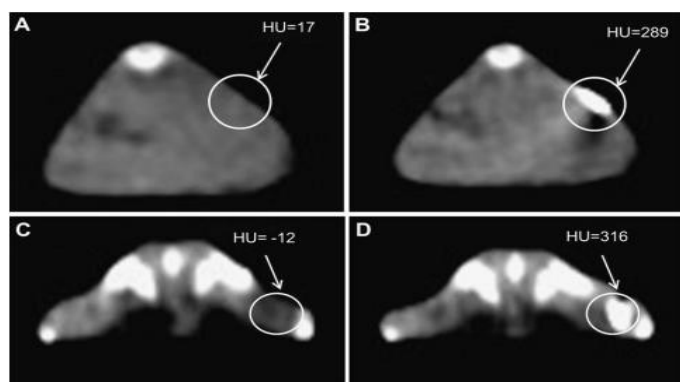


Figure 14: After injection of GNR-SiO₂-FA suspended in PBS, in vivo CT photographs of mice were taken. (A, B) The HU value of the injection site is 289 in the transverse image of the back; (C, D) the HU value of the injection site is 316 in the transverse image of the buttock. With permission from Ref. [46].

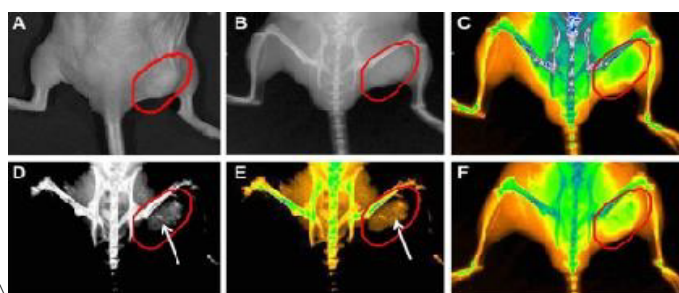


Figure 15: In vivo X-ray photographs of nude mice following intravenous injection of GNR-SiO₂-FA at various time points. (A) a photograph of tumor tissue; (B) an X-ray picture taken at 0 h, (C) an X-ray image taken at 0 h (in color), (D) an X-ray image taken at 12 h, (E) an X-ray image taken at 12 h (in color), and (F) an X-ray image taken at 24 h (in color). With permission from Ref. [46].

Figure 14. After injection of GNR-SiO₂-FA suspended in PBS, in vivo CT photographs of mice were taken. (A, B) The HU value of the injection site is 289 in the transverse image of the back; (C, D) the HU value of the injection site is 316 in the transverse image of the buttock. With permission from Ref. [46], this article has been reprinted.

An obvious image was observed 12 hours after intravenous injection of GNR-SiO₂-FA in naked mice filled with gastric cancer MGC803 cells at different time points (Figure 15).

In vivo X-ray photographs of nude mice following intravenous injection of GNR-SiO₂-FA at various time points. (A) a photograph of tumor tissue; (B) an X-ray picture taken at 0 h, (C) an X-ray image taken at 0 h (in color), (D) an X-ray image taken at 12 h, (E) an X-ray image taken at 12 h (in color), and (F) an X-ray image taken at 24 h (in color). With permission from Ref. [46], this article has been reprinted.

The researchers will agree on the above encounters, calculate the tumor size, and propose Methods for clinical trial therapy as a result of this X-ray image [46].

A study of silica nanoparticle for in vivo application

Park et al. recently developed luminescent porous silicon nanoparticles (LPSiNPs) (Figure 16). The drug release and cytotoxicity of DOX-loaded LPSiNPs were studied in vitro.

Figure 16. (a) Schematic diagram depicting the structure and in vivo degradation process of the silica NPs.

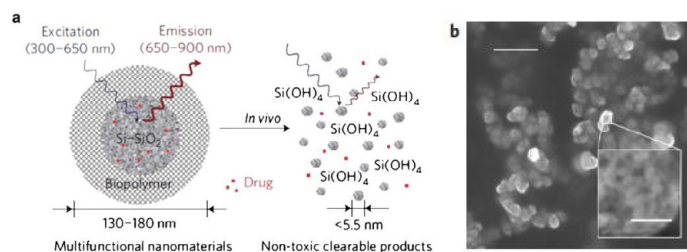


Figure 16. (a) Schematic diagram depicting the structure and in vivo degradation process of the silica NPs.

(b) SEM image of LPSiNPs. Reprinted with permission from Ref.[47]

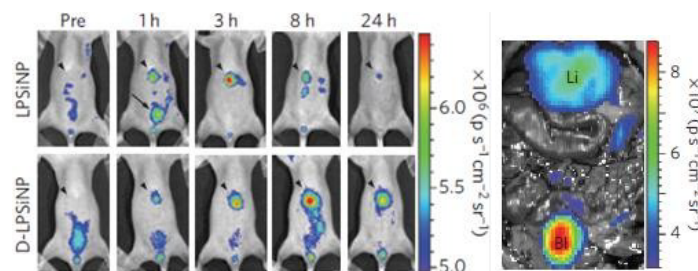


Figure 17. (a) LPSiNPs and D-LPSiNPs in vivo photographs After intravenous injection of LPSiNPs and D- LPSiNPs, the mice were imaged at various time points (20 mgkg⁻¹). The liver and bladder are shown by arrowheads and arrows with solid points, respectively. (b) In vivo picture 1 hour after injection showing the clearance of a portion of the ingested dose of LPSiNPs into the bladder. Liver is represented by the letters Li and Bl. With permission from Ref. [47], this article has been reprinted.

(b) SEM image of LPSiNPs. Reprinted with permission from Ref. [47]

Calcine was used to assess the viability of HeLa cells incubated with LPSiNPs at the specified concentrations for 48 hours. No cytotoxicity was observed at different doses of LPSiNPs. DOX molecules were transported to RES organs (e.g., liver and spleen) by LPS iNPs and were fully excreted from the body after 4 weeks.

Figure 17.a) LPSiNPs and D-LPSiNPs in vivo photographs After intravenous injection of LPSiNPs and D- LPSiNPs, the mice were imaged at various time points (20 mgkg⁻¹). The liver and bladder are shown by arrowheads and arrows with solid points, respectively. (b) In vivo picture 1 hour after injection showing the clearance of a portion of the ingested dose of LPSiNPs into the bladder. Liver is represented by the letters Li and Bl. With permission from Ref. [47], this article has been reprinted.

Fluorescence imaging of various organs (liver, spleen, kidney, lymph nodes, breast, bladder, lung, skin, and brain) was done 24 hours after injection, with the liver and spleen organs having the most biodistribution. LPSiNPs are a good choice for monitoring their biodistribution and degradation in living organisms because of their intrinsic luminescent properties.

CONCLUSION

Improvements in theranostics for cancer are definitely needed. Many drug potencies and therapeutic effects, for example, are diminished or otherwise diminished due to gradual decay that happens before they meet a targeted destination in the body; in most situations, prescription release has historically been diffusion-controlled until ingested, and time-dependent drug release provides patient continuity. We anticipate that the existing data on the biological effects of these nanomaterials in vitro and in vivo would need to be expanded in order to satisfy realistic clinical needs. The

chemical flexibility of these non-metallic nanomaterials would help these nanocarriers, allowing them to have clinically beneficial properties such as increased blood regulation, tumor specificity, biodegradability, and clearance from the human body. We assume they will be useful in theranostics in the future.

REFERENCES

1. Yu-Cheng Chen, Xin-Chun Huang, Yun-Ling Luo, Yung-Chen Chang, You-Zung et al. Non-metallic nanomaterials in cancer theranostics a review of silica- and carbon-based drug delivery systems. *Sci. Technol. Adv. Mater.* 2013;(14)044407(23pp).
2. Xu X, Ray R, Gu Y, Ploehn H J, Scrivens W A et al. Electrophoretic analysis and purification of fluorescent single-walled carbon nanotube fragments. *J. Am. Chem. Soc.* 126:12736-7.
3. Liu H, Ye T, Mao C. Fluorescent carbon nanoparticles derived from candle soot. *Angew. Chem. Int. Edn Engl.* 2007;46:6473-5.
4. Ray S C, Saha A, Jana N R, Sarkar R. Fluorescent carbon nanoparticles: synthesis, characterization, and bioimaging application. *J. Phys. Chem.* 2009; C11318546-51.
5. Kam N W S, Liu Z A, Dai H J. Carbon nanotubes as intracellular transporters for proteins and DNA: an investigation of the uptake mechanism and pathway. *Angew. Chem. Int. Edn Engl.* 2006;45:577-81.
6. Katz E, Willner I. Biomolecule-functionalized carbon nanotubes: applications in nanobioelectronics. *Chem Phys Chem.* 2004;5:1084-104.
7. Friebel M, Meinke M. Determination of the complex refractive index of highly concentrated hemoglobin solutions using transmittance and reflectance measurement. *J. Biomed. Opt.* 2005;10:064019.
8. Shi D, Guo Y, Dong Z, Lian J, Wang W et al. Quantum-dot-activated luminescent carbon nanotubes via nano scale surface functionalization for in vivo imaging. *Adv. Mater.* 2007;19:4033-7.
9. Welsher K, Liu Z, Daraciang D, Dai H. Selective probing and imaging of cells with single walled carbon nanotubes as near-infrared fluorescent molecules. *Nano Lett.* 2008;8:586-90.
10. de la Zerda A, Liu Z, Bodapati S, Teed R, Vaithilingam S et al. Ultrahigh sensitivity carbon nanotube agents for photoacoustic molecular imaging in living mice. *Nano Lett.* 2010;10:2168-72.
11. Guo Y. In vivo imaging and drugs to target by quantum-dot-conjugated carbon nanotubes. *Adv. Funct. Mater.* 2008;18:2489-97.
12. Hartman K B, Laus S, Bolskar R D, Muthupollai R, Helm LT et al. Gadonanotubes as ultrasensitive pH-smart probes for magnetic resonance imaging. *Nano Lett.* 2008;8:415-19.
13. Heister E, Neves V, Tilmaciu C, Lipert K, Beltran V S et al. Triple functionalisation of single-walled carbon nanotubes with doxorubicin, a monoclonal antibody, and a fluorescent marker for targeted cancer therapy. *Carbon. Nanobiotechnology.* 2009;4:72152-60.
14. Chen J, Chen S, Zhao X, Kuznetsova LV, Wong S S et al. Functionalized single-walled carbon nanotubes as rationally designed vehicles for tumor-targeted drug delivery. *J. Am. Chem. Soc.* 2009;130:16778-85.
15. Liu Z, Sun X, Ratchford N N, Dai H et al. Supramolecular chemistry on water-soluble carbon nanotubes for drug loading and delivery. *ACS Nano.* 2007;1:50-6.
16. Li R, Wu R, Zhao L, Wu M, Yang L et al. P-glycoprotein antibody functionalized carbon nanotube overcomes the multidrug resistance of human leukemia cells. *ACS Nano.* 2010;4:1399-408.
17. Ghosh S, Dutta S, Gnomes E, Carroll D, Jr R D et al. Increased heating efficiency and selective thermal ablation of malignant tissue with DNA-encased multiwalled carbon nanotubes. *ACS Nano.* 2009;3:3707-13.
18. Moon H K, Lee S H, Choi H C. In vivo near-infrared mediated tumor destruction by photothermal effect of carbon nanotubes. *ACS Nano.* 2009;3:3707-13.
19. Chakravarty P, Marches R, Zimmerman N S, Swafford A D, Bajaj P et al. Thermal ablation of tumor cells with antibody-functionalized single-walled carbon nanotubes. *Proc. Natl. Acad. Sci.* 2008;105:8697-702.
20. Dina G Zayed, Ahmed S Abdelhamid, May S Freag, Ahmed O Elzoghby. Hybrid quantum dot-based theranostic nanomedicines for tumor-targeted drug delivery and cancer imaging. *Nanomedicine (Lond).* 2019;14(3):225-228.
21. Volsi AL, Fiorica C, D'amico M. Hybrid Gold/Silica/Quantum-dots supramolecular nanostructures encapsulated in polymeric micelles as potential theranostic tool for targeted cancer therapy. *Eur. Polym. J.* 2018;105, 38-47.
22. Li S, Su W, Wu H. Targeted tumor theranostics in mice via carbon quantum dots structurally mimicking large amino acids. *Nat Biomed Eng.* 2020;(4)704-716.
23. Klingeler R, Hampel S, Buchner B. Carbon nanotube based biomedical agents for heating, temperature sensing and drug delivery. *Int J Hypertherm.* 2018;24:496-505.
24. Smith A.M, Duan H, Mohs A.M, Nie S. Bioconjugated quantum dots for in vivo molecular and cellular imaging. *Adv. Drug Deliv. Rev.* 2008;60:1226-1240.
25. Pan J, Feng S S. Targeting and imaging cancer cells by folate-decorated, quantum dots (QDs)-loaded nanoparticles of biodegradable polymers. *Biomaterials.* 2009;30:1176e83.
26. Kelkar S S, Reineke T M. Theranostics: combining imaging and therapy. *Bioconjug Chem.* 2011;(22)1879-1903.
27. Rahul S. Tade, Pravin O. Patil. Theranostic Prospects of Graphene Quantum Dots in Breast Cancer. *ACS Biomater Sci Eng.* 2020 Nov 9;6(11):5987-6008.
28. Vaishali Bagalkot, Liangfang Zhang, Etgar Levy-Nissenbaum. Quantum Dot-Aptamer conjugates for synchronous cancer imaging, Therapy, and Sensing of Drug Delivery based on Bi-Fluorescence Resonance Energy Transfer. *Nano Lett.* 2007;7(10):3065-70.
29. Nurunnabi M, Cho K.J, Choi J.S, Huh K.M, Lee Y.K et al. Targeted near-IR QDs-loaded micelles for cancer therapy and imaging. *Biomaterials.* 2010;(31)5436-5444.
30. Ibrahim Birma Bwatanglang, Faruq Mohammad. In vivo tumor targeting and anti-tumor effects of 5-fluorouracil loaded, folic acid targeted quantum dot system. *J. Colloid Interface Sci.* 2016;480:146-158.
31. Liu X, Tao H, Yang K, Zhang S, Lee S T, et al. Optimization of surface chemistry on single-walled carbon nanotubes for in vivo photothermal ablation of tumors. *Biomaterials.* 2011;32(1):144-51.
32. Yang W, Ratnac KR, Ringer SP, Thordarson P, Gooding J J, et al. Carbon nanomaterials in biosensors: should you use nanotubes or graphene? *Angew Chem Int Ed Engl.* 2010;15.49(12):2114-38.
33. Fatma Vatansever, Rakkayappan Chandran. Multi-Functionality in Theranostic Nanoparticles: is more Always Better? *J Nanomed Nanotechnol.* 2013;3(8).
34. Leeuw, T. K. Single-walled carbon nanotubes in the intact organism: near-IR imaging and biocompatibility studies in *Drosophila*. *Nano Lett.* 2007;7:2650-2654.
35. Kevin Welsher, Zhuang Liu, Sarah P. A route to brightly fluorescent carbon nanotubes for near-infrared imaging in mice. *Nature Nanotechnology.* 2009;4.
36. Yang S T, Luo J, Zhou Q, Wang H. Pharmacokinetics 2012 metabolism and toxicity of carbon nanotubes for biomedical purposes. *Theranostics.* 2012;2:271-282.

37. Liu Z, Fan A.C, Rakhra K, Sherlock S. Supramolecular stacking of doxorubicin on carbon nanotubes for in vivo cancer therapy. *Angew. Chem. Int. Ed Engl.* 2009;48.
38. Liu Z, Chen K, Davis C. Drug delivery with carbon nanotubes for in vivo cancer treatment, *Cancer Res.* 2009;686652-6660.
39. Liu Z, Davis C, Cai W, He L, Chen X et al. Circulation and long-term fate of functionalized, biocompatible single-walled carbon nanotubes in mice probed by Raman spectroscopy. *Proc. Natl Acad. Sci. USA* 2008;105.
40. Zhenjiang Zhang, Liming Wang, Jing Wang. Mesoporous Silica-Coated Gold Nanorods as a Light-Mediated Multifunctional Theranostic Platform for Cancer Treatment. *Adv. Mater.* 2012;(24)1418- 1423.
41. Jana N.R, Earhart C, Ying J.Y. Synthesis of water-soluble and functionalized nanoparticles by silica coating, *Chem. Mater.* 2007;19.
42. Ghanavi J, Mostafavi M, Ghanavi Z. Method for the synthesis of metallic nano products. US Patent 9,487,399, 2016.
43. Ghanavi J, Mostafavi M. Method for producing rod-shaped and branched metallic nano-structures by polyol compounds. US Patent. 20110088511.
44. Chen W, Xu N, Xu L. Multifunctional magnetoplasmonic nanoparticle assemblies for cancer therapy and diagnostics (theranostics). *Macromol Rapid Commun.* 2010;18;31(2):228-36.
45. Koole R, van Schooneveld M.M, Hilhorst J. Paramagnetic lipid-coated silica nanoparticles with a fluorescent quantum dot core: a new contrast agent platform for multimodality imaging. *Bioconjug Chem.* 2008;(19)2471-2479.
46. Peng Huang, Le Bao, Chunlei Zhang. Folic acid-conjugated Silica-modified gold nanorods for X-ray/CT imaging-guided dual-mode radiation and photo-thermal therapy. *Biomaterials* 2011;(32)9796-9809.
47. Ji-Ho Park, Luo Gu, Geoffrey von Maltzahn. Biodegradable luminescent porous silicon nanoparticles for in vivo applications. *Nat Mater.* 2009;8(4):331-6.